Int J Adv Manuf Technol (2013) 68:2085–2093
DOI 10.1007/s00170-013-4807-2

ORIGINAL ARTICLE

Simulation and assessment of diamond mill grinding wheel topography

Guochao Qiao · Guojun Dong · Ming Zhou

Received: 12 September 2012 / Accepted: 25 January 2013 / Published online: 14 February 2013

Abstract The topography of grinding wheel has a remarkable effect on grinding process. In this paper, the topographies of two mill grinding wheels with different grain sizes were measured by using an Olympus confocal scanning laser microscope. Kolmogorov–Smirnov normality tests were carried out to obtain distribution characteristics of abrasive grains. The test results indicate that the surface of grind wheel is of non-Gaussian nature. Consequently, a non-Gaussian statistical model was proposed to simulate the mill grinding wheel topography. Simultaneously, some parameters of "Birmingham 14" were introduced to assess the grinding wheel surface quantitatively. Simulated profile of the grinding wheel is found to correspond well in appearance with that of the actual grinding wheel.

Keywords Topography · Simulation · Assessment · Mill grinding wheel · Statistical model

1 Introduction

It is well known that the topography and structure of diamond grinding wheel strongly affect the machined surface quality in precision grinding [1–3]. However, it is difficult to characterize the topography of grinding wheel as abrasive grains of the wheel usually embed desultorily in metallic or resin bond, and the shapes of grains and spatial interval between grains are all random.

To overcome the problem, many researchers devoted special efforts to modeling and simulating of the topography of grinding wheel. These models can be clarified into two main types: empirical model and simulative model.

Empirical model, which is based on the measurement data from experiments, is the most direct method to acquire the topography of grinding wheel. All the measured data were inputted into computer, and a special procedure was performed to establish the topography of grinding wheel. Nowadays, there are many ways to measure the topography of grinding wheel. Based on the interaction mechanism, they can be classified into contact and noncontact methods [4]. The contacting technique essentially involves the use of a mechanical stylus and is based on the interaction mechanism of the measurement probe with the surface. The disadvantages of this technique are that high-frequency feature can be lost, and the stylus radius will widen the peak width while narrow and shallow the valley; at the same time, the wear of stylus will reduce the measurement precision. Noncontacting technique includes optical focus detection, optical interferometry, atomic force microscopy, light scattering, capacitance, and some varieties of scanning probe microscopy [5–7]. This kind of method has high precision and is easy to accomplish. But, both contact and noncontact techniques are all time-consuming to measure the whole wheel.

Simulative model is a statistical model based on the principle of statistics. This kind of model simulates the topography of grinding wheel based on the distribution characteristics of the grinding wheel acquired by Monte Carlo method. A variety of simulation models were reported in the last decades [8–10]. Zhou et al. [11] considered the

G. Qiao · G. Dong · M. Zhou (✉)
School of Mechanical and Electrical Engineering, Harbin Institute of Technology, P.O. Box 422, Harbin 150001, People's Republic of China
e-mail: zhouming@hit.edu.cn

G. Qiao
School of Mechanical and Electrical Engineering, Northeast Forestry University, Harbin 150040, China

random distribution of grains protrusion height as Gaussian distribution and established a predicted model of machined surface roughness. Koshy et al. [12, 13] and Zhen et al. [14] considered the abrasive grains as spheres and assumed that the grain's diameter is normally distributed, and the spatial distribution of abrasive grains is uniform in the wheel. Xie et al. [15] established a geometrical model to quantify the distribution of grain protrusion height. Lan et al. [16] studied the topography of Alumina grinding wheel and established a mathematical model of grain protrusion height. All these models suppose that grains' protrusion height of grinding wheel presents Gaussian distribution. But, in recent years, more and more researchers believe that grinding wheel surface is subject to non-Gaussian distribution [9, 17].

Up to now, there is no consensus about the distribution of the abrasive grain, which influences the accuracy of the simulation result of the grinding wheel topography tremendously. On the other hand, there are no accepted unified standard for assessing the topography of grinding wheel. These make it difficult to assess the topography of grinding wheel quantificationally.

In this work, the distribution information of abrasive grains of diamond mill grinding wheel is collected by using an Olympus confocal scanning laser microscope, and normality tests are carried out to verify the distribution characteristics. A statistical simulation model for non-Gaussian 3D surface is developed, and some parameters of Birmingham 14 are used to assess the mill grinding wheel topography. Simulation results are compared with the measured data to assess the validity of the proposed model.

2 Measurement of mill grinding wheel surface

2.1 Experimental conditions

Two metal-bonded diamond mill grinding wheels with different grain sizes were measured. The wheel denoted by Do.6-D76H has an average grain size of 76 μm and an outer diameter of φ6mm, while the average grain size and outer diameter of the wheel denoted by Do.12-D91H are 91 μm and φ12mm, respectively. The concentration of the two wheels is all 100 %. Experiments were performed by using an Olympus confocal scanning laser microscope (LEXT OLS3000), of which the moving resolution is 0.01 μm, the scale resolution is 5 nm, and the stroke is 10 mm in vertical direction. In order to eliminate the random error, four 1.28× 1.28-mm^2 areas on the wheel circumferential surface were chosen randomly as the measuring object, and the sampling interval is 1.25 μm in X and Y directions. Figure 1 shows one of the measurement locations and the SEM microphotograph of the wheel Do.6-D76H. The measured images of the two grinding wheels are shown in Fig. 2a, b.

2.2 Measurement data processing

It can be seen from Fig. 2 that the measured data of the grinding wheel surface include three types of signals: the distribution signal of abrasive grains, the curvature signal of the mill grinding wheel, and the white noise signal. In other words, the original measured data cannot reflect the characteristics of grinding wheel surface correctly unless they are processed appropriately. Therefore, some suitable data processing methods must be adopted to eliminate the disturbance signals.

Data processing in this work is divided into two steps. One step is to remove the wheel curvature component, and the other is to eliminate the influence of white noise. To remove the wheel curvature information from the original data, a least-squares second-order 3D surface polynomial fitting was performed. Once the fitting curved surface is confirmed, the curvature will be removed by subtracting fitting curved surface from original grinding wheel surface. The data fitting results of the two grinding wheels are shown in Fig. 3.

After removing the wheel curvature component from the original data, the data signals only contain low-frequency component and high-frequency component. The former describes the characteristics of grinding wheel surface, while the latter represents the white noise. The existence of high-frequency noise confuses extremely the characteristic signals of the grinding wheel; therefore, this must also be eliminated.

In this paper, power spectral density (PSD) method was adopted to analyze the residual surface signal. A forward Fourier transform was performed to transform time domain signal into frequency domain signal. The PSD graphs of the grinding wheels are shown as Fig. 4. It can be seen from Fig. 4 that the value of PSD decreases sharply with an increase in spatial frequency, and once the frequency exceeds a certain value (called cutoff frequency), the value of PSD attenuates to zero. For Do.6-D76H wheel, the cutoff frequency is 0.14 μm^{-1}, while for Do.12-91H, the frequency is 0.125 μm^{-1}.

Once the cutoff frequency was obtained, an ideal low-passed filtering was performed to remove the noise. Furthermore, the inverse Fourier transform was carried out to recover the time domain signal, and a MATLAB program was compiled to plot the topography of mill grinding wheels as shown in Fig. 5.

The function of power spectral density P_{PSD} could be expressed in Eq. (1) as follows:

$$P_{\mathrm{PSD}}(f) = \frac{1}{N}\left|\sum_{n=1}^{N}\eta(x,y)e^{-j2\pi(n-1)f}\right|^2 \tag{1}$$

where N is the total number of the sampling data points, j is the imaginary unit, and f is the spatial frequency.

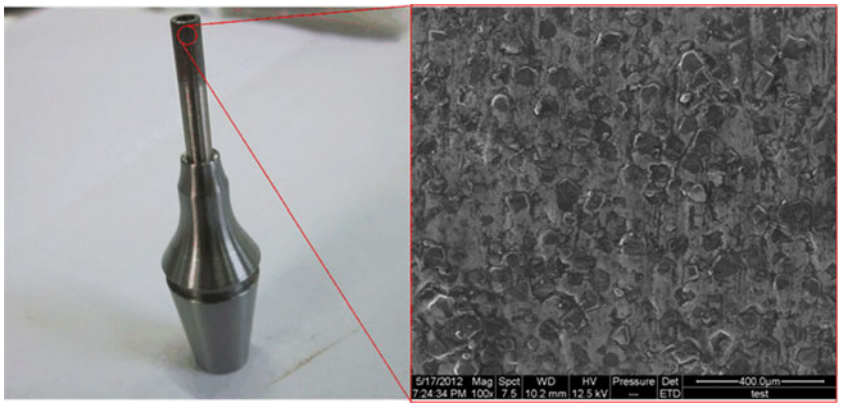

Fig. 1 The metal-bonded diamond mill grinding wheel

3 Simulation of mill grinding wheel topography

3.1 Normality tests for grains protrusion heights

After the measurement data were filtered, the following task is to confirm the distribution characteristics of abrasive grains. It is difficult to distinguish grains from the bond as abrasive grains embed in grinding wheel surface randomly. In this paper, eight nearest neighbor criterion was adopted to define grain. When the height of a point is higher than the heights of eight nearest neighbor points, the point is defined as the grain.

In order to confirm the probability distribution of mill grinding wheel surface, Kolmogorov–Smirnov normality tests were carried out for the two grinding wheels respectively. The test results indicate that the P values are all far less than 0.05. For Do.6-D76H wheel, skewness is −0.651, and kurtosis is 4.3,

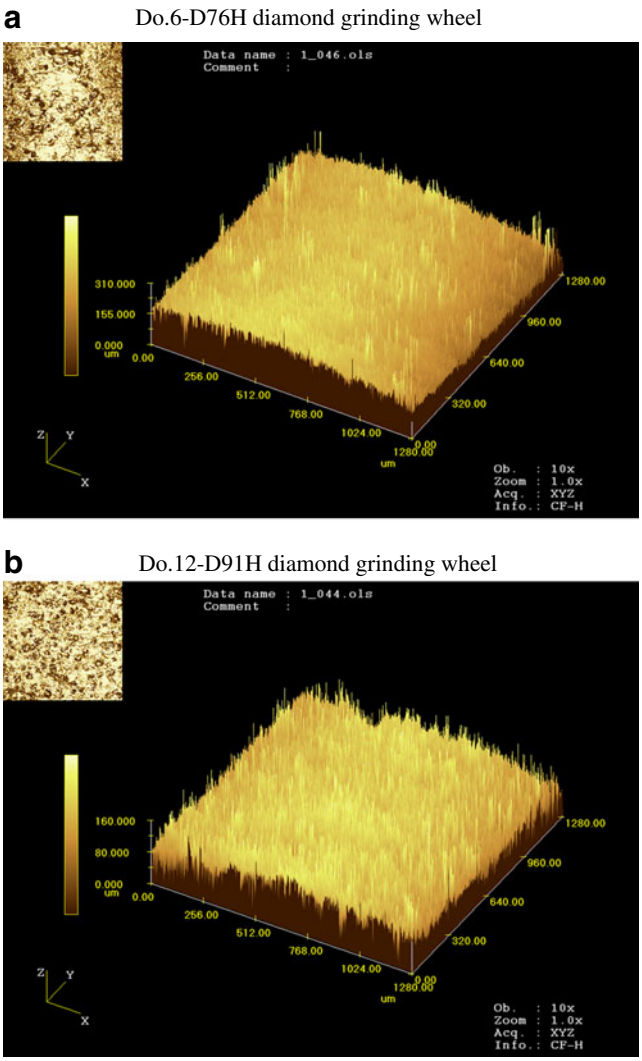

Fig. 2 Measured topography of grinding wheels **a** Do.6-D76H diamond grinding wheel. **b** Do.12-D91H diamond grinding wheel

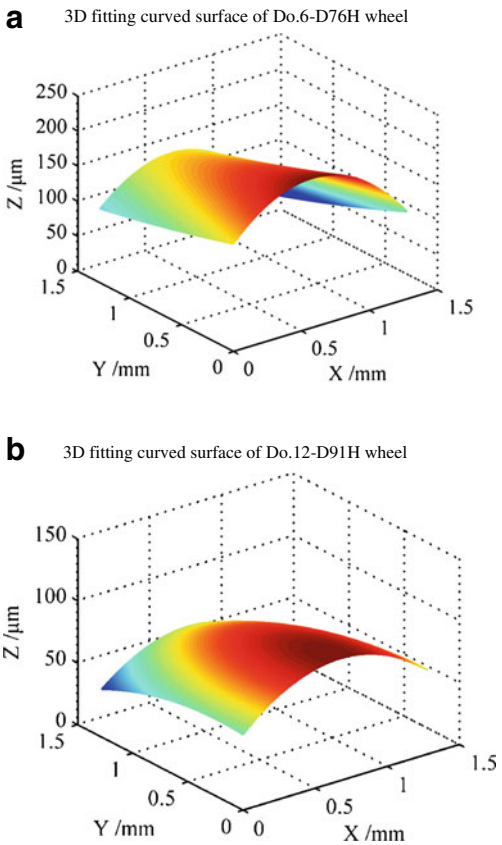

Fig. 3 Fitting results of the two grinding wheels. **a** 3D fitting curved surface of Do.6-D76H wheel; **b** 3D fitting curved surface of Do.12-D91H wheel

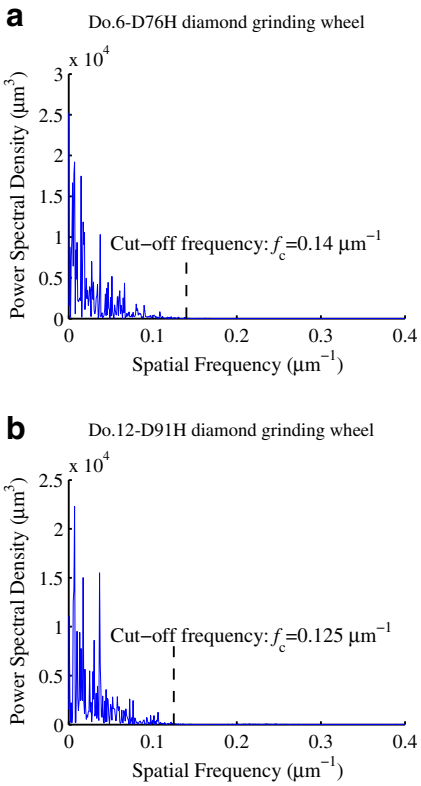

Fig. 4 Power spectral density of the mill grinding wheel. **a** Do.6-D76H diamond grinding wheel. **b** Do.12-D91H diamond grinding wheel

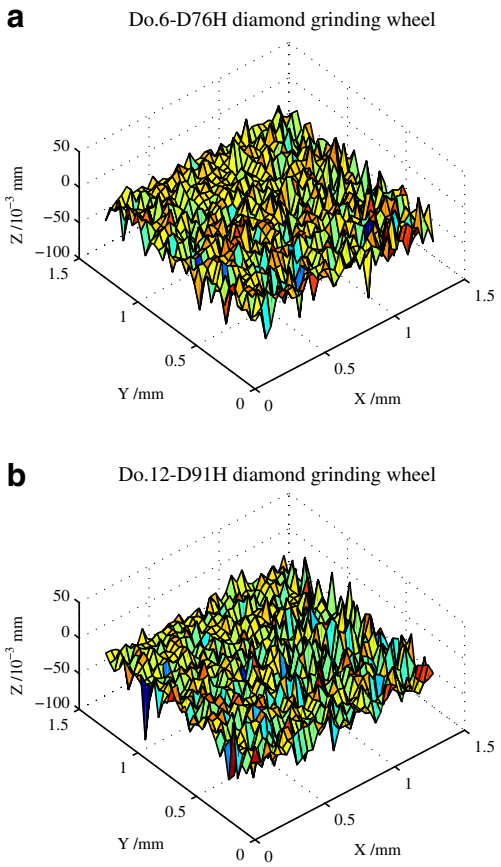

Fig. 5 Measured surface topography of grinding wheels. **a** Do.6-D76H diamond grinding wheel. **b** Do.12-D91H diamond grinding wheel

while for Do.12-D91H wheel, they are −4.18 and 1.015, respectively. All these parameters verified that the samples are non-Gaussian distribution. In order to illustrate it more clearly, the histogram and Q–Q plots of the two wheels are shown in Fig. 6.

3.2 Johnson transform system

For Gaussian distribution field, it is easily to generate a set of random numbers subject to a certain mean and standard deviation by Gaussian probability density function. For non-Gaussian field, however, it cannot produce a series of random numbers directly, because the probability density function is unknown.

There are two available methods to simulate non-Gaussian field: one is transforming a non-Gaussian field to a designed Gaussian ones which has the same probabilistic characteristics, for example, Johnson transform, and the other is simulating directly by replacing the driver Gaussian white noise with non-Gaussian noise in the spatial series. In this work, the Johnson transform method is adopted.

Johnson transform system can be generally described by Eq. (2) as follows:

$$Z = \gamma + \delta f\left(\frac{X-\varepsilon}{\lambda}\right) \tag{2}$$

where Z is a standard normal variable, and X is a variable with a non-Gaussian distribution. Parameters γ and δ determine the shape of the distribution X, while ε and λ are location and scale factors, respectively.

According to different values of skewness (S_k) and kurtosis (K_u), the transform system can be divided into three formations as shown by Eqs. (3) and (5).

The bounded system (S_B)

$$Z = \gamma + \delta \ln\left(\frac{X-\varepsilon}{\varepsilon+\lambda-X}\right) \tag{3}$$

The unbounded system (S_U)

$$Z = \gamma + \delta \sinh^{-1}\left(\frac{X-\varepsilon}{\lambda}\right) \tag{4}$$

The lognormal system (S_L)

$$Z = \gamma + \delta \ln\left(\frac{X-\varepsilon}{\lambda}\right) \tag{5}$$

The parameters of the Johnson transform system can be computed by statistic software or MATLAB procedure. In

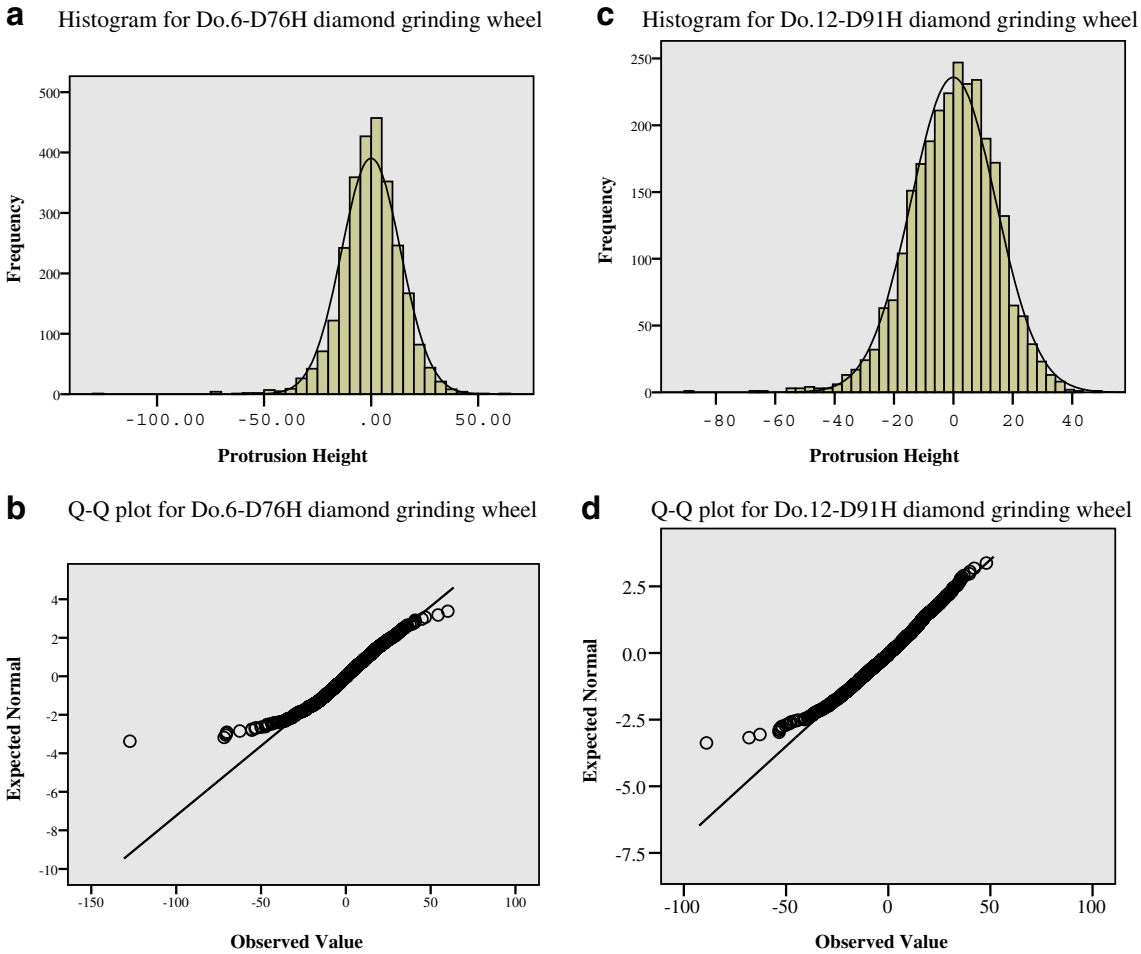

Fig. 6 Histograms and Q–Q plots of Kolmogorov–Smirnov normality tests. **a** Histogram for Do.6-D76H diamond grinding wheel. **b** Q–Q plot for Do.6-D76H diamond grinding wheel. **c** Histogram for Do.12-D91H diamond grinding wheel. **d** Q–Q plot for Do.12-D91H diamond grinding wheel

this work, the statistic software Minitab 15 was used to calculate the parameters.

Through calculation, the unbounded system (S_U) is found suitable for both Do.6-D76H and Do.12-D91H wheels. Consequently, their expressions could be rearranged as Eqs. (6) and (7), respectively.

$$Z = 0.173843 + 1.92728 \sin h^{-1}\left(\frac{X - 2.39095}{22.5134}\right) \quad (6)$$

$$Z = 2.47985 + 4.87674 \sin h^{-1}\left(\frac{X - 32.9491}{60.6712}\right) \quad (7)$$

3.3 Simulation of mill grinding wheel topography

Through Johnson transform, a normal matrix was attained which can describe the distribution characteristics of the original non-Gaussian matrix. In other word, the non-Gaussian 3D surface of mill grinding wheel can be simulated by two parameters through inverse Johnson transform. The two parameters are mean (μ) and standard deviation (σ) of the normal matrix, respectively. Based on the analysis mentioned above, the topographies of the two mill grinding wheels were simulated as shown in Fig. 7.

4 Evaluation of the mill grinding wheel topography

How to assess a 3D surface is always an issue. Traditionally, 2D parameters, such as R_a and R_z, are widely used to assess machined surface quality, but these parameters cannot supply enough information to characterize a 3D surface. Despite the efforts of many researchers to define 3D parameters for general use, there is still no accepted standard for 3D characterization. In Europe, 14 parameters proposed by the University of Birmingham have been widely adopted by the research community. These parameters so-called "Birmingham 14" include amplitude, spatial, hybrid, and functional parameters [4]. In this work, some of them were used to assess the mill grinding wheel topography.

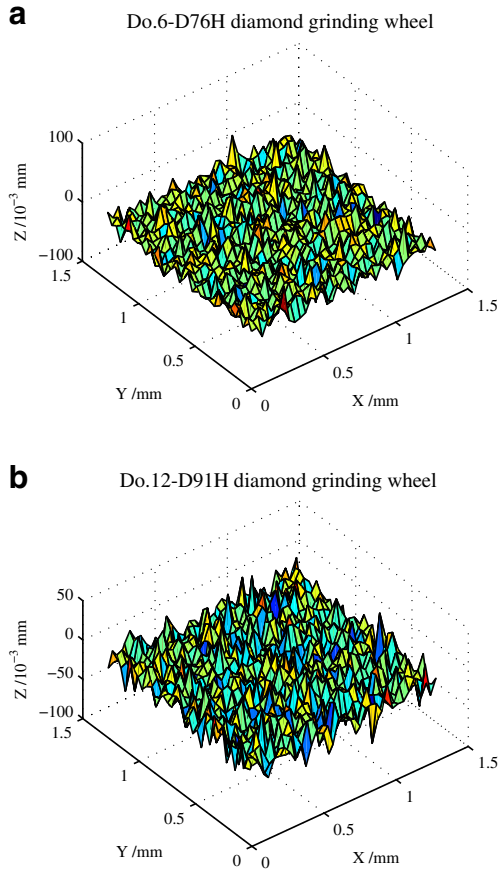

Fig. 7 Generated topography of grinding wheel by Johnson transform. **a** Do.6-D76H diamond grinding wheel. **b** Do.12-D91H diamond grinding wheel

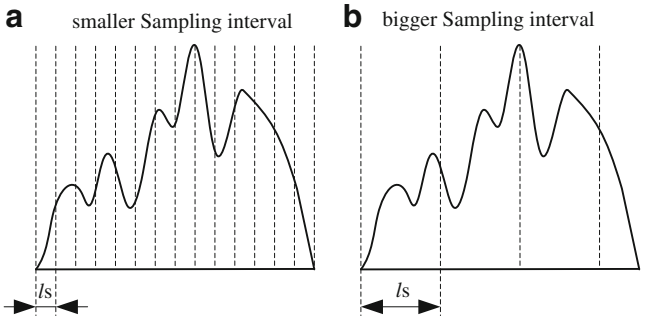

Fig. 8 The effect of different sampling intervals on the number of summit

4.1 The density of abrasive grains

Because grains embed in mill grinding wheel surface randomly, it is impossible to describe the distribution feature of abrasive grain precisely. Birmingham 14 defined the average density of summits of the sampling area to describe the density of abrasive grains of grinding wheel as Eq. (8).

$$S_{ds} = \frac{n}{(M-1)(N-1)\cdot \Delta x \cdot \Delta y} \tag{8}$$

where n is the number of summits, M is the number of points of per profile, N is the number of profiles, and Δx and Δy are the sampling interval in x and y direction, respectively.

From the definition, it can be seen that the key problem is how to select the suitable sampling interval. Figure 8 illustrates the effect of sampling interval on the density of abrasive grains intuitively. Since different sampling intervals will produce diverse results, it is necessary to select an appropriate sampling interval for different mill grinding wheel.

It is well known that sampling frequency should abide by the Nyquist sampling principle. In addition, Blunt [18] suggested that a suitable sampling interval should meet the equation expressed as follows:

$$\frac{d}{4} \le l_s \le \frac{d}{3} \tag{9}$$

where d is the diameter of abrasive grain, and l_s is the sampling interval.

According to this criterion, in this paper, sampling interval of 20 and 26 μm were adopted for Do.6-D76H and Do.12-D91H wheels, respectively. In addition, another important thing should be noted is that S_{ds} must be assessed after Wolf pruning at 5 % of S_z. S_z is the maximum height of the topography surface. In other words, only 5 % of the maximum values of S_z can be defined as summit.

4.2 The amplitude feature of abrasive grain

In Birmingham 14, root-mean-square deviation (S_q), average amplitude (S_a), and maximum height of the topography surface (S_z) are the most frequently used parameters to characterize the amplitude feature of the surface. They are defined by Eqs. (10) and (12).

$$S_q = \left[\frac{1}{MN}\sum_{j=1}^{N}\sum_{i=1}^{M}\eta^2(x_i, y_j)\right]^{\frac{1}{2}} \tag{10}$$

$$S_a = \left[\frac{1}{MN}\sum_{j=1}^{N}\sum_{i=1}^{M}\left|\eta(x_i, y_j)\right|\right]^{\frac{1}{2}} \tag{11}$$

$$S_z = \left|\max\left(\eta_p\right)\right| + \left|\min(\eta_v)\right| \tag{12}$$

where $\eta(x, y)$ is the residual surface, and η_p and η_v are the highest peak and lowest valley, respectively, as illustrated in Fig. 9.

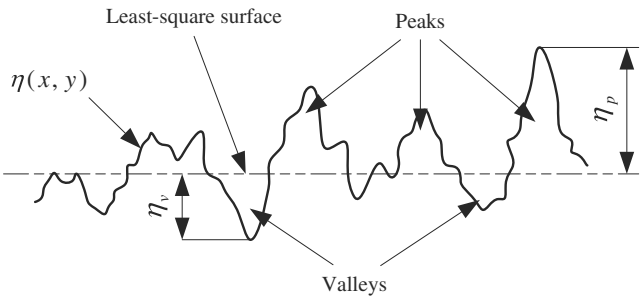

Fig. 9 The sketch diagram of one surface profile

These parameters describe the amplitude property of mill grinding wheel surface. The higher the value of the parameters is, the rougher the grinding wheel surfaces are.

4.3 The shape of abrasive grain

Abrasive grains have various irregular shapes, and it is impossible to describe the real shape of grains. Generally, simplified models are used to substitute real grains during the investigation of grinding, and they can be classified into three types: pyramid, cone, and hemisphere, as shown in Fig. 10. These types were used in different situations for a special purpose. In order to confirm the shape of grain, scanning electron microscope was used to observe the grains of diamond mill grinding wheel (Do.6-D76H), and the micrograph is shown in Fig. 11.

It can be seen clearly from Fig. 11 that most grains are pyramidal, and the tips of the pyramid are not absolutely sharp. In this paper, the pyramid model as shown in Fig. 10a was used to simplify the abrasive grain. Therefore, the shape of grain can be quantified by the radius of the spherical crown and the apex angle of the pyramid.

In Birmingham 14, arithmetic mean summit curvature S_{sc} and root-mean-square slope $S_{\Delta q}$ were defined to describe the average curvature and slope of summits. Their definitions were expressed by Eqs. (13) and (14), respectively.

$$S_{sc} = -\frac{1}{2} \cdot \frac{1}{n} \sum_{k=1}^{n} \left(\frac{\partial \eta^2(x,y)}{\partial x^2} + \frac{\partial \eta^2(x,y)}{\partial y^2} \right) \tag{13}$$

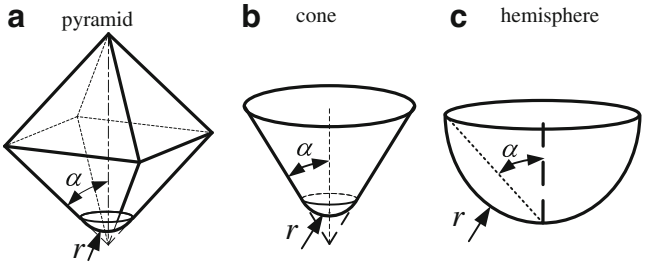

Fig. 10 Various simplified models of abrasive grain

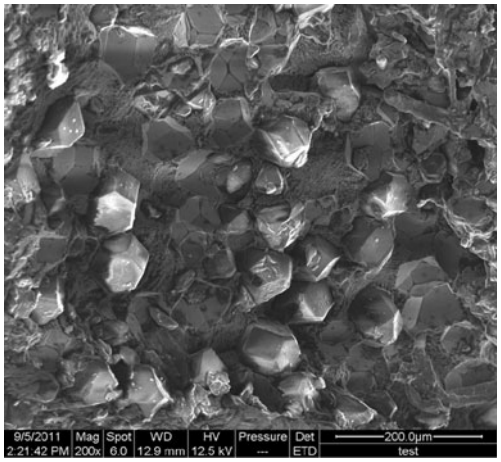

Fig. 11 Micrograph of grains of diamond grinding wheel

$$S_{\Delta q} = \left[\frac{1}{(M-1)(N-1)} \sum_{j=2}^{N} \sum_{i=2}^{M} \rho_{ij}^2 \right]^{\frac{1}{2}} \tag{14}$$

where

$$\rho_{ij} = \left[\left(\frac{\partial \eta(x,y)}{\partial x} \right)^2 + \left(\frac{\partial \eta(x,y)}{\partial y} \right)^2 \right]^{\frac{1}{2}} \tag{15}$$

The radius of spherical crown can be calculated by Eq. (16).

$$r = \frac{1}{S_{sc}} \tag{16}$$

Because most of grains have negative rake, the apex angle of grain can be calculated by Eq. (17).

$$2\theta = \pi - 2S_{\Delta q} \tag{17}$$

All calculated results of these parameters for Do.6-D76H and Do.12-D91H wheels are shown in Table 1.

Table 1 3D parameters of measured and simulated

Parameters	Do.6-D76H		Do.12-D91H	
	Measured	Simulated	Measured	Simulated
S_z (μm)	117.25	117.68	136.18	135.83
S_q (μm)	13.80	13.62	14.16	14.17
S_a (μm)	3.21	3.20	3.35	3.34
S_{ds} (mm^{-2})	14.95	16.97	9.40	9.40
S_{sc} (mm^{-1})	87.11	86.81	73.47	73.64
$S_{\Delta q}$ (°)	58.47	61.91	53.84	53.76
r (μm)	11.48	11.52	13.61	13.58
2θ (°)	63.06	56.18	72.32	72.48

5 Results and discussions

The simulated topography generated by the proposed model is similar in appearance with the measured topography as shown in Fig. 12. In order to verify further the consistency of the measured and simulated topography of mill grinding wheel quantitatively, 3D parameters defined above are calculated, and the results are listed in Table 1. The values of simulated parameters agree well with those of the measured parameters.

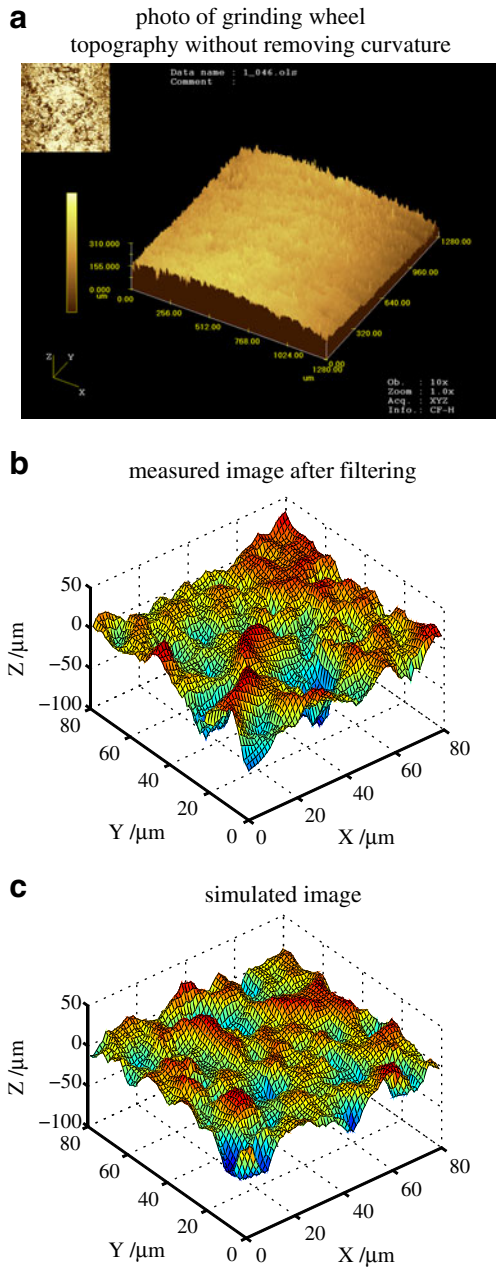

Fig. 12 Comparison between measured and simulated topographies of Do.6-D76H wheel. **a** Photo of grinding wheel topography without removing curvature, **b** measured image after filtering, **c** simulated image

The areal autocorrelation function (AACF) for measured and simulated grinding wheel topography was also estimated. Figure 13 shows the AACF of Do.12-D91H wheel. The difference between the AACFs for measured and simulated profiles is less than 0.2. These give a support to the validity of the proposed approach. Although the simulated topography is similar in appearance with the measured topography, there are still some deviations between measuring and

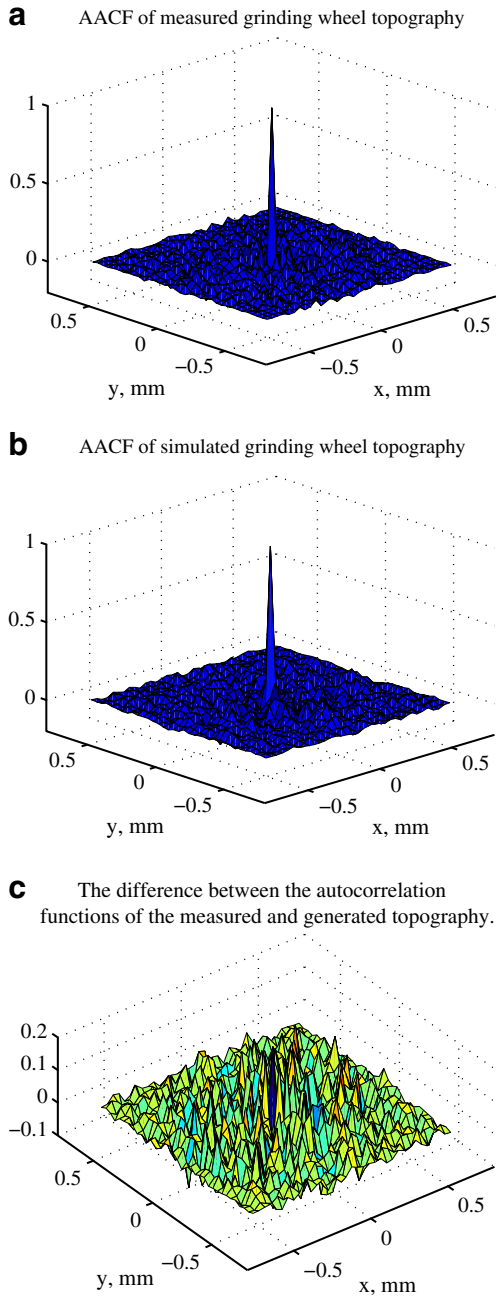

Fig. 13 Areal autocorrelation function of measured and generated topography of Do.12-D91H. **a** AACF of measured grinding wheel topography. **b** AACF of simulated grinding wheel topography. **c** The difference between the autocorrelation functions of the measured and generated topography

simulation results. These deviations mainly arise from measurement errors. Further research is still needed to improve the simulation accuracy of the proposed approach.

6 Conclusions

The surface topographies of two mill grinding wheels with different grain sizes were measured, and Kolmogorov–Smirnov normality tests were carried out to obtain distribution characteristics of abrasive grains. The test results indicate that mill grinding wheel surface exhibit non-Gaussian characteristics. A non-Gaussian statistical model was proposed to simulate the mill grinding wheel topography. The simulated topography generated by the proposed model was found similar in appearance with the measured topography. Some 3D parameters of Birmingham 14 are introduced to assess the mill grinding wheel surface quantitatively. The values of simulated parameters agree well with those of the measured parameters. The areal autocorrelation functions for measured and simulated grinding wheel topography were also estimated. The difference between the AACFs for measured and simulated profiles is less than 0.2. Further research is still needed to improve the simulation accuracy of the proposed approach.

Acknowledgments This work is partly supported by the National High-Tech R&D program (863 Program) of China (grant no. 2012AA040405) and the National Natural Science Foundation of China (grant no. 51075094).

References

1. Brecher C, Schug R, Weber A, Wenzel C, Hannig S (2010) New systematic and time-saving procedure to design cup grinding wheels for the application of ultrasonic-assisted grinding. Int J Adv Manuf Technol 47(1):153–159
2. Chen J, Huang H, Xu X (2009) An experimental study on the grinding of alumina with a monolayer brazed diamond wheel. Int J Adv Manuf Technol 41(1):16–23
3. Horvath M, Kundrak J, Mamalis A, Gyani K (2002) On the precision grinding of advanced ceramics. Int J Adv Manuf Technol 20(4):255–258
4. Mainsah E, Greenwood JA, Chetwynd DG (2001) Metrology and properties of engineering surfaces. Kluwer, Norwell, MA
5. Myshkin N, Grigoriev AY, Chizhik S, Choi K, Petrokovets M (2003) Surface roughness and texture analysis in microscale. Wear 254(10):1001–1009
6. Inasaki I (1996) Grinding process simulation based on the wheel topography measurement. CIRP Ann Manuf Technol 45 (1):347–350
7. Mathia T, Pawlus P, Wieczorowski M (2011) Recent trends in surface metrology. Wear 271(3):494–508
8. Doman DA, Warkentin A, Bauer R (2006) A survey of recent grinding wheel topography models. Int J Mach Tool Manuf 46 (3–4):343–352
9. Nguyen T, Butler D (2005) Simulation of precision grinding process, part 1: generation of the grinding wheel surface. Int J Mach Tool Manuf 45:1321–1328
10. Gong YD, Wang B, Wang WS (2002) The simulation of grinding wheels and ground surface roughness based on virtual reality technology. J Mater Process Tech 129(1–3):123–126
11. Zhou X, Xi F (2002) Modeling and predicting surface roughness of the grinding process. Int J Mach Tool Manuf 42(8):969–977
12. Koshy P, Jain VK, Lal GK (1997) Stochastic simulation approach to modelling diamond wheel topography. Int J Mach Tool Manu 37 (6):751–761
13. Koshy P, Ives LK, Jahanmir S (1999) Simulation of diamond-ground surfaces. Int J Mach Tool Manu 39(9):1451–1470
14. Hou ZB, Komanduri R (2003) On the mechanics of the grinding process—part I. Stochastic nature of the grinding process. Int J Mach Tool Manuf 43(15):1579–1593
15. Xie J, Xu J, Tang Y, Tamaki J (2008) 3D graphical evaluation of micron-scale protrusion topography of diamond grinding wheel. Int J Mach Tool Manuf 48(11):1254–1260
16. Lan Y, Rong FJ (2011) Quantitative evaluation and modeling of Alumina grinding wheel surface topography. Chin J Mech Eng 47 (17):179–186 (in Chinese)
17. Chen D, Tian Y (2010) Modeling and simulation methodology of the machined surface in ultra-precision grinding. Chin J Mech Eng 46(13):186–191 (in Chinese)
18. Blunt L, Ebdon S (1996) The application of three-dimensional surface measurement techniques to characterizing grinding wheel topography. Int J Mach Tool Manuf 36(11):1207–1226